Journal of Magnetism and Magnetic Materials 339 (2013) 157–162

Contents lists available at SciVerse ScienceDirect

Journal of Magnetism and Magnetic Materials

journal homepage: www.elsevier.com/locate/jmmm

Review

Intrinsic magnetic properties of $Bi_xCo_{2-x}MnO_4$ spinels obtained by short-time etching

M.E. dos Santos [a,b,*], P.N. Lisboa-Filho [c], F. Gouttefangeas [b], O. Peña [b]

[a] Grupo de Materiais Avançados, UNESP—Universidade Estadual Paulista, 17033-360 Bauru, SP, Brazil
[b] Institut des Sciences Chimiques de Rennes, UMR 6226, Université de Rennes, 135042 Rennes, France
[c] Departamento de Física, Faculdade de Ciências, Universidade Estadual Paulista, 17033-360 Bauru, SP, Brazil

ARTICLE INFO

Article history:
Received 11 December 2012
Received in revised form
22 January 2013
Available online 19 March 2013

Keywords:
Multiferroics
Oxide spinel
Ferrimagnetism
Etching
pH

ABSTRACT

We report the structural and magnetic properties of Co_2MnO_4, partially substituted by Bi at the octahedral site. Bismuth enhances ferromagnetism due to a decrease of the Co^{2+}–Co^{2+} antiferromagnetic interactions and an increase of the Mn^{3+}–Mn^{4+} exchanges. Spurious phases (magnetic and/or nonmagnetic oxides) can easily form because of the large differences between the ionic radii of Bi^{3+} and Co^{3+}, hiding or altering the intrinsic physical properties of the main $Bi_xCo_{2-x}MnO_4$ phase. An easy way to eliminate the secondary phases is using acid reagents. Short-time etching of $Bi_{0.1}Co_{1.9}MnO_4$ using nitric acid was successfully used, keeping most of the properties of the initial compound, with no alteration of the crystallographic structure. Final stoichiometry was respected ($\sim Bi_{0.08}Co_{1.82}MnO_4$), meaning that the material after etching definitely contains bismuth elements in its structure and the observed properties are intrinsic to the oxide spinel. Additional experiments were performed as a function of the synthesis conditions, showing that an optimal pH value of 7 allowed the best magnetic response of the non-doped material.

1. Introduction

Mixed-valence manganese oxides have played an important role on the understanding of magnetism and electricity in functional materials and multiferroic compounds [1]. Among these oxides, the Co_2MnO_4 spinel exhibits a rich variety of crystallographic, electronic and magnetic properties due to the mixed-valence of both the Co and Mn elements [2,3]. According to the arrangement of the crystallographic structure, the $Co^{2+}/Co^{3+}/Co^{III}$ (Co^{III} being the low-spin LS nonmagnetic state of cobalt) and $Mn^{2+}/Mn^{3+}/Mn^{4+}$ ions can be randomly distributed over the tetrahedral and octahedral positions [4], showing either a normal or an inverse spinel structure or even an intermediate distribution, all of them being represented by the formula $(A_{1-i}B_i)[A_iB_{2-i}]O_4$ (where i is the inversion parameter). The Co_2MnO_4 compound is an inverse spinel with a cationic arrangement represented by $(Co)[CoMn]O_4$ and for this reason we shall adopt from here on, the notation Co_2MnO_4 (instead of the more usual one for spinels, i.e. $MnCo_2O_4$).

Keeping in mind the conditions for multiferroïsme (transition metal with empty d-orbital and noncentrosymmetricity of a nonmagnetic ion [5]), doping the Co_2MnO_4 spinel with the bismuth element may enhance its physical properties since bismuth has empty d shells (d^0) and usually shifts away from the center of the oxygen polyhedra [6,7]. In the system under investigation, $Bi_xCo_{2-x}MnO_4$, the Bi^{3+} ion substitutes Co^{3+} at the octahedral site, inducing a valence fluctuation of both Co and Mn cations [8,9]. As a result, the magnetic properties will be modified, in particular, the antiferromagnetic Co^{2+}–Co^{2+} interactions at the tetrahedral sites will be reduced while the ferromagnetic interactions due to the double-exchange Mn^{3+}–Mn^{4+} will be enhanced [10].

Considering the large difference in ionic radii between Bi^{3+}(1.17 Å), Co^{3+}(0.65 Å) and Mn^{3+}(0.78 Å), the preparation of $Bi_xCo_{2-x}MnO_4$ represents a challenge from a crystallographic point of view since spurious phases, like BiO or Bi_2O_3, are easily formed, resulting in non-stoichiometric materials, eventually leading to the formation of some cobalt oxides if stoichiometry is not respected. Many approaches have been used to obtain polycrystalline spinel materials, like Co_2MnO_4. Methods such as combustion synthesis, sol–gel, co-precipitation, mechanosynthesis, solid-state reaction, etc., are normally employed [11,12]. However, incorporation of the bismuth element may become quite difficult mainly because of its volatility and the enormous difference in ionic radius compared to the substituted elements. In the present study, $Bi_xCo_{2-x}MnO_4$ materials, with $x=0.0$ and 0.1, were synthesized by a soft route based on a modified polymeric precursors

* Corresponding author at: Institut des Sciences Chimiques de Rennes, UMR 6226, Université de Rennes 1, 35042 Rennes, France. Tel.: +33 2 23 23 67 57; fax: +33 2 23 23 67 99.
E-mail addresses: e.santos@fc.unesp.br, elenice.dos-santos@univ-rennes1.fr (M.E. dos Santos).

0304-8853/$ - see front matter © 2013 Elsevier B.V. All rights reserved.
http://dx.doi.org/10.1016/j.jmmm.2013.02.047

method [13]; however, the X-ray data showed for $x=0.1$, the presence of a minimal BiO secondary phase. In order to minimize or get rid of such spurious phase(s), etching procedures have been widely reported in the literature, in particular in the case of the $BiFeO_3$ perovskite, allowing the removal of Bi-rich parasitic phases while keeping the crystallographic structure of the main phase with no changes. Following this idea, we performed the etching of the $Bi_{0.1}Co_{1.9}MnO_4$ sample using concentrated HNO_3 acid, during different times [14]. Results obtained after etching showed that the secondary phases are dramatically reduced, without destroying the main phase if this process is run for short times [15]. Our structural studies together with the magnetic characterization showed that this etching procedure is a suitable approach to eliminate magnetic and/or nonmagnetic spurious phases, thus having access to the intrinsic properties of the main material.

Prior to these investigations, we performed a systematic research on the optimal synthesis conditions employed in the soft chemistry route. For this, we focused on the non-doped system, Co_2MnO_4, modifying the pH environment from acid to basic and found that a pH value of 7 allowed obtaining upgraded magnetic response.

2. Experimental section

Polycrystalline Co_2MnO_4 and $Bi_{0.1}Co_{1.9}MnO_4$ samples were prepared by a modified polymeric precursors method [13]. Appropriate stoichiometric mixtures of Bi_2O_3 (Aldrich > 99.9% purity), CoO (Aldrich > 99.9% purity), MnO (Aldrich > 99% purity) were dissolved in water by adding HNO_3 (purity—15.2 mol/L, Aldrich > 99.9%) and a hydrocarboxylic acid ($C_6H_8O_7$—Aldrich > 99.9%) as a chelating agent. Ethylene glycol ($C_2H_6O_2$—Aldrich > 99.9%) was added at a temperature of 90 °C in a chelating/alcohol mass ratio of 60/40 to form the polymeric resin. In order to get optimal conditions regarding acidity, several tests were performed incorporating various quantities of ethylenediamine ($C_2H_8N_2$, Aldrich > 99.9%), reaching pH values comprised between 1 and 7. Based on the magnetic data obtained in these samples, a pH adjustment of 7 was adopted and kept as optimal for both the non-doped and Bi-doped samples (Co_2MnO_4 and $Bi_{0.1}Co_{1.9}MnO_4$, respectively). In order to eliminate the organic components, pyrolisis was performed at 400 °C for 4 h, followed by annealings at 850 °C—24 h, 1000 °C—12 h and 1100 °C—12 h, with intermediate grinding; finally, samples were slowly cooled at a suitable predefined rate. Presence of some impurities in the $Bi_{0.1}Co_{1.9}MnO_4$ compound led us to perform etching attacks for various times. For this, the powder sample was immersed in HNO_3 acid, in a 1/10 ratio acid-to-water, and kept for 30 min, 5 h and 15 h, following the procedure given in Ref. [15]. The leached samples were then dried at 400 °C for 4 h.

X-Ray diffraction (XRD) data were obtained on a Bruker D8 Discover diffractometer with Cu-$K_{\alpha 1}$ radiation ($\lambda=1.5418$ Å). Samples were indexed in the space group *Fd3m*. Scanning electron microscopy (SEM) images and X-ray energy dispersion spectra (EDS) were acquired with a JEOL JSM 6400 equipped with an OXFORD detector. Magnetic measurements were performed in a Quantum Design MPMS-XL5 SQUID magnetometer. Magnetization data were collected between 5 K and 400 K, under different applied fields (100 Oe for *ZFC/FC* cycles and 10 kOe for measurements in the paramagnetic state). Magnetization $M(H)$ loops were recorded at 10 K between −50 kOe and 50 kOe.

3. Results and discussion

3.1. Search of the optimal pH synthesis conditions

Several conditions of acidity were investigated by varying the content of ethylenediamine incorporated to the polymeric resin. Fig. 1 shows the magnetic properties of a Co_2MnO_4 material prepared under conditions of pH=1 and pH=7. By looking at the FC magnetization extrapolated at $T=0$ (Fig. 1a) together with the value of the magnetization obtained at 50 kOe (Fig. 1b), it becomes quite obvious that a pH of 7 is the most favorable condition to upgrade the magnetic properties of the material, even though the coercive field (value of the magnetic field when $M=0$) appears diminished with increasing pH. All these data will be discussed in Section §0.3.3, together with the presentation of the magnetic results obtained for the Bi-doped material, before and after leaching by an acid reagent.

3.2. Structural and microstructural aspects

By adopting the synthesis conditions described above, a new series of samples of the $Bi_xCo_{2-x}MnO_4$ series was prepared, from $x=0$ up to $x=0.3$. For simplicity, we will refer from here on, only to samples with $x=0$ and 0.1, since our goal is to describe the effects of etching on the physicochemical properties of the material (for a full description of the doping effects, see Ref. [10]).

Fig. 2 presents the XRD patterns of Co_2MnO_4 and $Bi_{0.1}Co_{1.9}MnO_4$, collected in a continuous mode in the 2θ range (10°-85°) with a 0.02° step. Co_2MnO_4 crystallizes in the cubic spinel structure with space group *Fd3m* ($Z=8$) (*JCPDS-ICDD* card no. 84-0482) and exhibits the corresponding crystallographic planes given in Fig. 2. A similar pattern, with well-defined peaks corresponding to the crystallographic planes of the *Fd3m* cubic spinel structure, was obtained for the $Bi_{0.1}Co_{1.9}MnO_4$ sample. The insert, Fig. 2, zooms the data of the substituted sample in the range 27–42°. Substituting Bi^{3+} for Co^{3+} in $Bi_xCo_{2-x}MnO_4$ leads to an increase of the cell parameter a (8.271 Å and 8.283 Å for Co_2MnO_4 and $Bi_{0.1}Co_{1.9}MnO_4$, respectively), correlated with the fact that the substituting element (Bi^{3+}) has a larger ionic radius (1.17 Å) than Co^{3+}

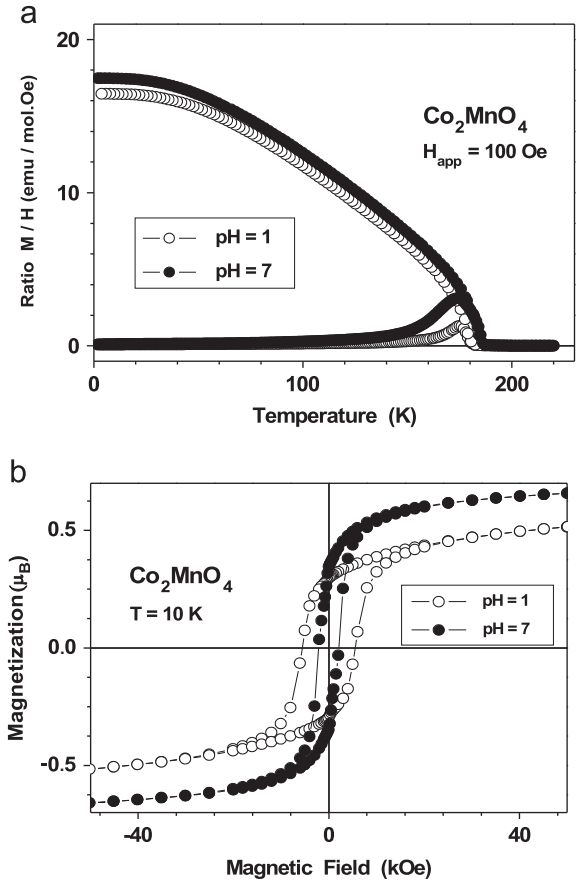

Fig. 1. Co_2MnO_4 materials prepared under conditions of pH=1 (open symbols) and 7 (closed symbols): (a) ZFC/FC cycles and (b) magnetization loops.

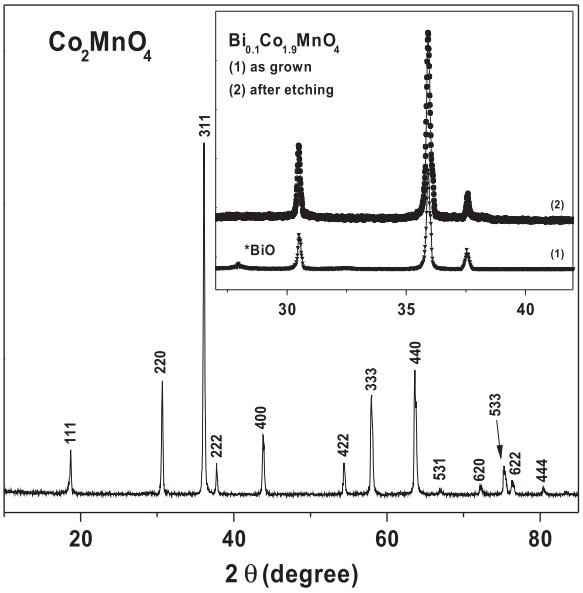

Fig. 2. X-ray diffraction, Cu-$K_{\alpha 1}$, $\lambda = 1.5418$ Å, for Co_2MnO_4 heat-treated at 1100 °C for 12 h, indexed in a cubic spinel *Fd3m* (227) space group. Inset: XRD data of $Bi_{0.1}Co_{1.9}MnO_4$, before (1) and after etching (2), zoomed in the range 27–42° (asterisk symbol * shows the BiO impurity present in the as-grown sample).

(0.65 Å). In addition, distortions of the oxygen octahedra and a Jahn–Teller effect associated to the Mn^{3+} ion are expected in the $x = 0.1$ material, which will induce important modifications to the antiparallel alignment of the Co^{2+} spins, as it will be discussed later [16,17]. No spurious phases were found in the XRD pattern of Co_2MnO_4; however, minute amounts of BiO oxide (peak marked ∗ in the insert of Fig. 2) were observed for $x = 0.1$. Considering the large difference between ionic radii of Bi and Co and the low-temperature soft-synthesis route employed in this study, Bi-oxide phases are easily formed relative to the main phase [18].

In order to eliminate such BiO impurities, portions of the $Bi_{0.1}Co_{1.9}MnO_4$ sample were etched by using concentrated nitric acid HNO_3. Several tests at different time intervals and/or varying the H_2O/HNO_3 ratio were carried on $Bi_{0.1}Co_{1.9}MnO_4$ samples initially containing BiO. It was found that the most appropriate conditions to fully eliminate the secondary phase, without destroying the material, corresponded to a 30-minutes etching in a solution of 1/10: HNO_3/H_2O ratio. Under these conditions, the peaks belonging to the BiO phase have completely disappeared, as shown in the insert of Fig. 2. Prolonging the reaction time ended up with a segregated amorphous material, with no diffraction lines on the XRD data and quite obvious secondary phases on the magnetic response, as it will be shown later.

Fig. 3 presents the SEM micrographs of the Co_2MnO_4 and $Bi_{0.1}Co_{1.9}MnO_4$ samples. The non-doped material, Co_2MnO_4 (Fig. 3a), shows a uniform morphology, with grains of relatively regular shape and homogeneously distributed over the surface, even though large agglomerations appear occasionally; no spurious phases were observed, confirming our XRD results. The Bi-doped Co_2MnO_4 showed similar grain morphology before etching but traces of impurities, represented by the white spots in Fig. 3b and identified as a bismuth oxide, appeared at the grain boundaries of the main phase.

After etching, the SEM micrograph of the $Bi_{0.1}Co_{1.9}MnO_4$ phase showed negligible quantities of white spots, indicating that leaching the material with HNO_3 acid is a very suitable and powerful method to dissolve the parasitic BiO phase (Fig. 3c). It is important to remark that the grain morphology of the etched sample has radically changed compared to the non-etched sample. Indeed, once all the BiO disappeared at the grain boundaries, the aggregates break up and a large number of smaller grains are formed.

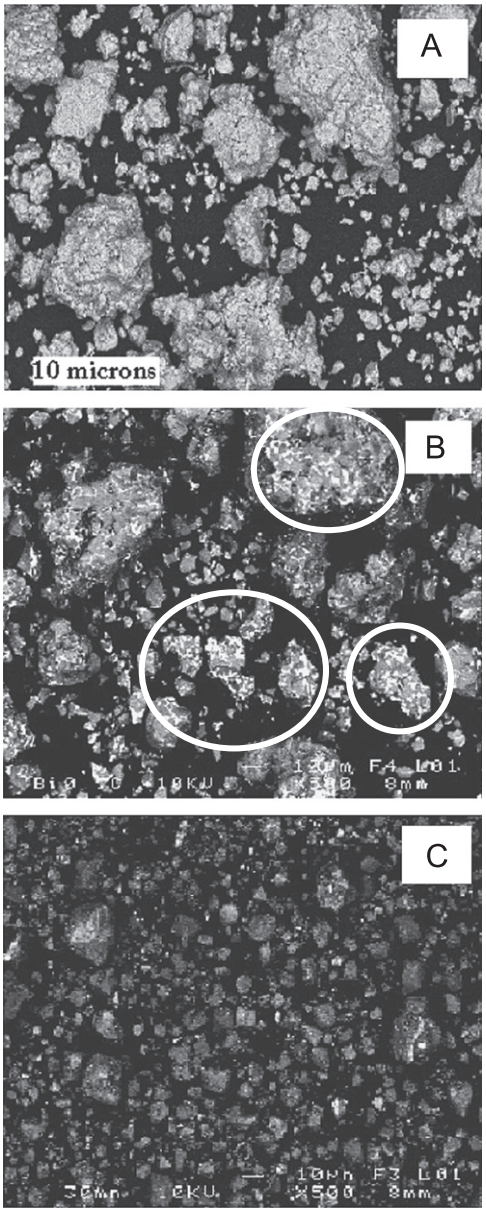

Fig. 3. Scanning electron microscopy (SEM) images for Co_2MnO_4 and (a) $Bi_{0.1}Co_{1.9}MnO_4$ before (b) and after etching (c). Circles in (b) enhance the presence of white spots identified as bismuth oxide impurities.

From Fig. 3b and c, the average grains sizes were evaluated to 48.2 and 6.3 μm for samples before and after 30-minutes etching, respectively. This disaggregation process continues and becomes very important at longer etching times (5 and 15 h), turning the powder into an amorphous material with no XRD footprints, as pointed out above.

X-ray energy dispersive (EDX) analyses allowed evaluating the final compositions for each sample, compared to the nominal ones. Values obtained were: $Co_{1.9738}Mn_{1.0272}O_4$, $Bi_{0.0853}Co_{1.8508}Mn_{1.1339}O_4$ and $Bi_{0.0802}Co_{1.8171}Mn_{1.1821}O_4$ for, respectively, Co_2MnO_4, $Bi_{0.1}Co_{1.9}MnO_4$ and the etched sample $Bi_{0.1}Co_{1.9}MnO_4$. Several comments can be made on these results. Firstly, the nominal and experimental compositions of the pristine material are quite in agreement, within the experimental uncertainties. Secondly, the bismuth contents ($Bi_{0.0853}$ and $Bi_{0.0802}$) of the doped materials are rather low and deviate from the expected value ($x = 0.1$) due to the formation of some bismuth oxide phase. Thirdly, the bismuth content after etching decreases by about 6% with respect to the non-etched sample, showing the effects

of the etching procedure, not only to get rid of the BiO impurities but also leaching some of the Bi atoms incorporated in the structure. It is important to stress, however, that all magnetic properties discussed here below, related to the etched sample, definitely correspond to the intrinsic behavior of a Bi-doped Co_2MnO_4 spinel. Finally, we shall notice that the content of cobalt is also reduced by about 2% in the etched sample ($Co_{1.8508}$ and $Co_{1.8171}$), a fact which will have important consequences on the paramagnetic moment, as we will discuss later.

3.3. Magnetic properties

Magnetic measurements were performed both as a function of temperature and field. Figs. 1a and 4a show the zero-field-cooled/field-cooled (ZFC/FC) cycles, measured under an applied field of 100 Oe in the temperature range [2–220 K], for the three samples under investigation: Co_2MnO_4 for pH=7 (Fig. 1a) and the Bi-doped materials $Bi_{0.1}Co_{1.9}MnO_4$ before and after etching (Fig. 4a). Magnetization loops were performed at $T=10$ K, with varying applied fields, from +50 kOe down to −50 kOe, and back again (Figs. 1b and 4b). Additional measurements were performed in the range [200–400 K], under an applied field of 10 kOe (Fig. 5) to evaluate the effective moment. Magnetic parameters obtained through these various techniques are given in Table 1.

Considering the thermal variation of the $M(T)$ magnetization (ZFC/FC cycles), it is quite evident that two magnetic contributions coexist: an antiferromagnetic-like interaction, evidenced by the peak shape of the *ZFC* magnetizations and by the highly negative Curie–Weiss temperatures Θ_{cw} obtained in these materials (Table 1 and Ref. [10]) and a ferromagnetic interaction, evidenced by the abrupt increase of the *FC* magnetization at the ordering temperature T_C. The ferromagnetic component is specially seen in the magnetization loops $M(H)$, characterized by large coercive fields H_C and by the rapid increase of the magnetization at low fields, almost reaching a saturation regime above $H\sim20$ kOe.

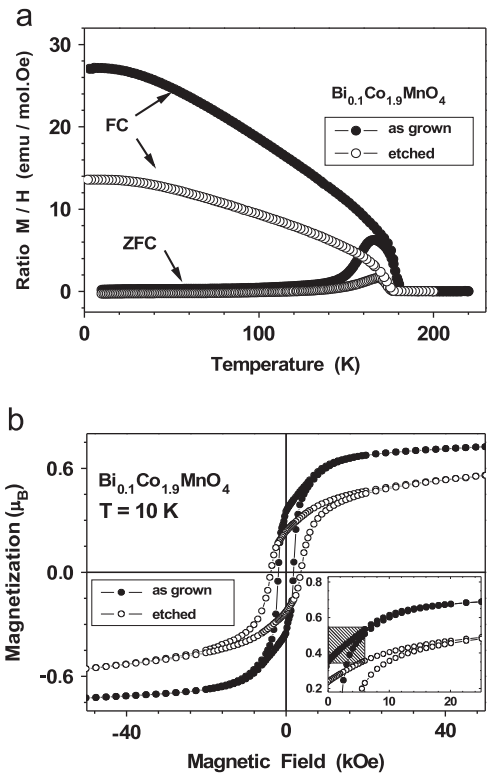

Fig. 4. Magnetic behavior of $Bi_{0.1}Co_{1.9}MnO_4$, before (closed circles) and after 30-minutes etching (open circles): (a) ZFC/FC cycles and (b) magnetization loops. Inset highlights the anomalous contribution due to BiO impurities present in the as-grown sample (hatched area).

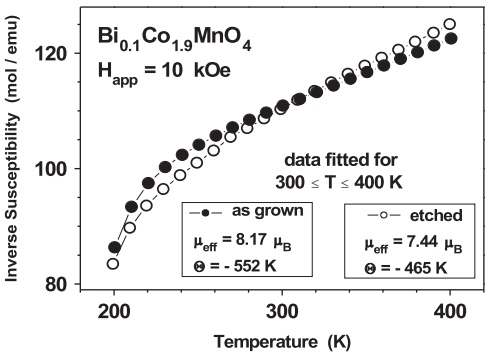

Fig. 5. Inverse magnetic susceptibility of $Bi_{0.1}Co_{1.9}MnO_4$, before (closed circles) and after 30-minutes etching (open circles). Data was fitted by a Curie–Weiss expression in the range 300–400 K.

3.3.1. As grown samples

It is clear that the presence of bismuth, a nonmagnetic ion, changes the interactions of the magnetic cations, namely, Co and Mn elements. It is interesting to notice, indeed, that the value of the magnetization M_{FC} extrapolated to $T=0$, increases by about 50% when the initial material Co_2MnO_4 contains 10 at% Bi in the octahedral site. A similar enhancement of the ferromagnetic properties is observed in the value of the magnetization $M_{50\ kOe}$ taken at 50 kOe (from 0.66 μ_B to 0.72 μ_B, for Co_2MnO_4 and $Bi_{0.1}Co_{1.9}MnO_4$, respectively). To understand such behavior we have to recall the main mechanisms of magnetic interactions existing in these spinels, namely the J_{AA}, J_{BB} and J_{AB} intrasite and intersite exchange between sublattices A and B [10]. From these, the most relevant to our study are the antiferromagnetic Co^{2+}–Co^{2+} interactions at tetrahedral positions and the ferromagnetic Mn^{3+}–Mn^{4+} interactions at octahedral positions, both of them intrasite exchange. Less important are the intersite J_{AB} between Co^{2+}–Mn^{3+} and Co^{2+}–Mn^{4+}. When replacing part of the cobalt ions by bismuth, the antiferromagnetic interactions associated to the cobalt sublattice are reduced because of the spin canting induced by the octahedral distortions, favoring the ferromagnetic component and an enhanced ferromagnetism.

It is also interesting to notice the subtle changes in the ZFC magnetization near the ferromagnetic transition. By carefully looking at the ZFC peaks, one can notice that Co_2MnO_4 shows a narrow and asymmetric peak, with a maximum value at $T=T_{max}=175$ K (Fig. 1a), whereas the $x=0.1$ sample, before etching, exhibits a wide maximum at $T=T_{max}=166$ K, with a quite symmetric variation (Fig. 4a). It is probable that the presence of BiO at the grain boundaries creates additional stresses to the lattice, enlarging the antiferromagnetic-like variation of the ZFC magnetization.

3.3.2. Etching effect

Several effects are worth noticing with regard to etching. First of all, we should call the attention to an anomalous behavior in the $M(H)$ loop of the non-etched Bi-substituted $Bi_{0.1}Co_{1.9}MnO_4$ sample: a spurious contribution of approximately 20% of the saturation moment is noticed in the insert, Fig. 4b (hatched area below 6 kOe), usually seen in all samples containing bismuth, whereas in the case of Co_2MnO_4 (Fig. 1b), the variation of $M(H)$ at low fields is quite smooth. This spurious contribution disappears completely with etching (open symbols, insert of Fig. 4b), resulting again in a smooth variation of M(H) at low fields. It is interesting to notice that the "saturation" magnetization (magnetization measured at

Table 1
Magnetic parameters for $Bi_xCo_{2-x}MnO_4$ ($x=0.0$ synthesized under pH=7 conditions, $x=0.1$ before etching, $x=0.1$ after etching). T_C: Transition temperature, T_{max}: temperature values at the *ZFC* magnetization peaks, Θ_{CW}: Curie–Weiss temperatures, μ_{eff}: effective moments, H_C: coercive fields values, M_{FC}: extrapolation of FC curves at $T=0$, $M_{50\ kOe}$: magnetization measured at $H=50$ kOe. Final compositions obtained by EDX analysis are also given.

$Bi_xCo_{2-x}MnO_4$	EDX analysis	T_C (K)	T_{max} (K)	Θ_{CW} (K)	μ_{eff} (μ_B)	H_C (Oe)	M_{FC} ($T=0$) (emu/mol)	$M_{50\ kOe}$ (μ_B)
0.0 (pH=7)	$Co_{1.974(2)}Mn_{1.027(2)}MnO_4$	185	175	−630	8.2	2100	17.5	0.66
0.1 as-grown	$Bi_{0.085(2)}Co_{1.851(2)}Mn_{1.134(1)}MnO_4$	181	166	−552	8.2	1850	27.2	0.72
0.1 after etching	$Bi_{0.080(2)}Co_{1.817(2)}Mn_{1.182(1)}MnO_4$	176	168	−465	7.4	3730	13.6	0.56

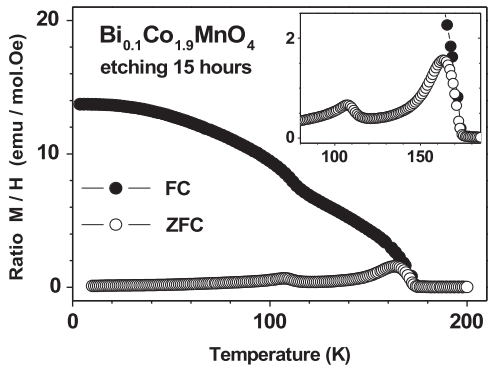

Fig. 6. Temperature dependence of a $Bi_{0.1}Co_{1.9}MnO_4$ sample, etched for longer times (15 h), under the same water-to-acid conditions as for the 30-minutes etching. Notice the appearance of a magnetic transition at ~110 K due to partial decomposition.

our highest applied fields) decreased by an equivalent amount (20%), showing once again the close correlation between the presence of BiO and the occupation of the tetrahedral and octahedral sites by the magnetic Co and Mn ions.

Etching affects the coercive field of these materials through shape and size effects, as seen in Fig. 4b. As shown in the SEM micrographs, Fig. 3c, aggregates break up under the action of the acid reagent and grains dramatically decrease in size. As a result, the size of the magnetic domains decreases and the number of pinning centers at the origin of the coercive field increases, ending up with a factor of 2 between the coercive field H_C of the as-grown and the etched samples (1.85 kOe and 3.73 kOe, respectively). Etching also affects the shape of the ZFC maximum since, as discussed above, presence of BiO at the grain boundaries creates additional distortions to the lattice. So, by eliminating such strains at the boundaries, the ZFC magnetization recovers its original shape, with a narrow and asymmetric peak centered at $T=T_{max}=168$ K.

We should also mention the consequences of etching on the paramagnetic moment. As mentioned above, about 2% of the initial cobalt content was leached away by the acid solution, together with 6% of the bismuth atoms inserted in the structure. This effect is clearly seen through the evaluation of the effective moment, for which the inverse susceptibility was fitted in the range [300–400 K] by a classical Curie–Weiss law $\chi = C/T-\theta_{CW}$ (Fig. 5). The as-grown specimens (Co_2MnO_4 and $Bi_{0.1}Co_{1.9}MnO_4$) gave a similar magnetic moment of 8.2 μ_B, which has been interpreted by the substitution of the non-magnetic low-spin Co^{III} ion by non-magnetic Bi^{3+}, in such a way that the magnetic contributions of each one of the magnetic ions Co^{2+}, Co^{3+}, Mn^{3+} and Mn^{4+} compensate each other [10]. After leaching part of the cobalt atoms, the paramagnetic moment decreases to 7.4 μ_B whereas the Curie–Weiss temperature increases from −552 K up to −465 K after etching (Table 1).

Finally, a warning should be made on the effects of prolonged etching. Tests performed for 5 and 15 h, under the same conditions of acid reagent, ended up with amorphous powder samples, with no XRD signals. However, the crystallographic spinel phase was not completely destroyed by such hard and strong attack, since the magnetic ZFC/FC cycle showed the expected ferromagnetic transition at about 174 K accompanied by a second transition centered at 107 K (Fig. 6), whose origin could not be determined through our XRD or EDS observations.

4. Conclusions

We showed that polycrystalline samples of $Bi_xCo_{2-x}MnO_4$ ($x=0.0$ and 0.1) can be prepared using a soft route based on a modified polymeric precursors method. Optimum synthesis conditions were found for a pH equals to 7. From the analysis of the XRD data it was seen, however, that a single phase was difficult to form in the case of Bi-substituted samples ($Bi_{0.1}Co_{1.9}MnO_4$) due to the large difference between the ionic radii of Bi^{3+} and Co^{3+}. The magnetic properties are enhanced with the bismuth-presence; however, this enhancement is partially due to a BiO spurious phase existing at the grains boundaries, which creates additional distortions, provokes canting of the antiparallel-aligned Co^{3+} spins and enhances the ferromagnetic component. A short-time etching by concentrated nitric acid allows to eliminate the BiO secondary phases, although it leaches away part of the bismuth and cobalt atoms inserted in the structure. Through the EDX analysis we showed that the Co_2MnO_4 spinel contains non-negligible amounts of Bi in its structure and thus, the magnetic properties herein reported are definitely intrinsic to the Bi-doped $Bi_{0.08}Co_{1.82}MnO_4$ material.

Acknowledgments

Authors are thankful to FAPESP Grant 2007/08072-0. Authors also acknowledge the bilateral exchange program France-Brazil CAPES-COFECUB, Project no. 706/11. M.E. dos Santos in a Joint Ph. D. International Program, UNESP-Université de Rennes 1.

References

[1] M.B. Salamon, M. Jaime., Modern Physics Letters 73 (2001) 583.
[2] P.A. Joy, S.K. Date, Journal of Magnetism and Magnetic Materials 210 (2001) 31.
[3] S. Guillemet-Fritsch, C. Tenailleau, H. Bordeneuve, A. Rousset., Advances in Science and Technology 67 (2010) 143.
[4] E. Ríos, P. Lara, D. Serafini, A. Restovic, J.L. Gautier., Journal of the Chilean Chemical Society 55 (2010) 261.
[5] N.A. Spaldin, S. Cheong, R. Ramesh., Physics Today 63 (10) (2010) 38.
[6] E.A.V. Ferri, I.A. Santos, E. Radovanovic, R. Bonzanini, E.M. Girotto., Journal of the Brazilian Chemical Society 19 (6) (2008) 1153.
[7] N.E. Rajeevan, R. Kumar, D.K. Shukla, P. Thakur, N.B. Brookes, K.H Chae, W. K. Choi, S. Gautam, S.K. Arora, I.V. Shvets, P.P Pradyumnan., Journal of Physics: Condensed Matter 21 (2009) 406006.
[8] R. Kumar, S.K. Arora, I.V. Shvets, N.E. Rajeevan, P.P. Pradyumnan, D.K. Shukla., Journal of Applied Physics 105 (2009) 07D910.
[9] B.L. Ahuja, A. Dashora, N.L Heda, S. Tiwari, N.E Rajeevan, M. Itou, Y. Sakurai, R. Kumar., Applied Physics Letters 97 (2010) 212502.
[10] M.E. dos Santos, R.A. Ferreira, P.N. Lisboa-Filho, O. Peña., Journal of Magnetism and Magnetic Materials 329 (2013) 53.
[11] N.E. Rajeevan, P.P. Pradyumnan, R. Kumar, D.K. Shukla, S. Kumar, A.K. Singh, S. Patnaik, S.K. Arora, I.V. Shvets., Applied Physics Letters 92 (2008) 102910.
[12] A.L. Heck, S.R. Taffarel, R. Hoffmann, U.L. Portugal Jr., S.L. Jahn, E.L. Foletto, Ceramics 51 (2005) 117.
[13] M. Motta, C.V. Deimling, M.J. Saeki, P.N. Lisboa-Filho, Journal of Sol-Gel Science and Technology 46 (2008) 201.

[14] Q. Jiang, C. Nan, Y. Wang, Y. Liu, Z. Shen, Journal of Electroceramics 21 (2008) 690.
[15] E.S. Bickford, S. Velu, C. Song, Preprints of Papers-American Chemical Society, Division of Fuel Chemistry 49 (2) (2004) 649.
[16] R. Epherre, C. Pepin, N. Penin, E. Duguet, S. Mornet, E. Pollert, G. Goglio, Journal of Materials Chemistry 21 (2011) 14990.
[17] A. Moure, T. Hungría, A. Castro, J. Galy, O. Peña, I. Martínez, J. Tartaj, C. Moure, Ceramics International 38 (2012) 1507.
[18] N.E. Rajeevan, R. Kumar, D.K. Shukla, P.P. Pradyumnan, S.K. Arora, I.V. Shvets, Materials Science and Engineering B 163 (2009) 48.